AIAA JOURNAL
Vol. 45, No. 9, September 2007

Study of the Effect of Glow Discharges Near a $M = 3$ Bow Shock

P.-Q. Elias* and B. Chanetz†
ONERA, 92190 Meudon, France
and
S. Larigaldie‡ and D. Packan§
ONERA, 91761 Palaiseau, France

DOI: 10.2514/1.28515

This paper aims at investigating the effect of discharges generated near steady bow shocks and their possible use for localized heat deposition leading to drag reduction. We report the observation of steady discharges generated in front of a blunted model in a $M = 3$ supersonic flow. The test model is designed as a pair of coaxial electrodes, and set up in the ONERA R1Ch $M = 3$ blowdown wind tunnel. A high voltage power supply is used to generate negative discharges. A corona regime, a glow regime, and a filamentary arc regime are observed. The negative corona regime consists of Trichel pulses dissipating less than 200 mW of electrical power. The glow discharge absorbs powers up to 0.5 kW. It displays a strong light emission in the vicinity of the shock front, followed by a darker region downstream of the shock. The drag coefficient is measured and shows no measurable change when a glow discharge is switched on. To explain this and further investigate the effect of localized heat deposition at the shock front, modified Rankine–Hugoniot jump relations are computed, taking into account a volumetric heat source. This allows one to compute a fair estimate of the drag coefficient and shows that drag reduction by localized heating in the shock front is possible. However, it also shows that in our experiment, the plasma thermal power is too small to appreciably reduce the drag, possibly because of the role of the electron impact excitation of N_2 vibrations, whose fairly long relaxation time could shift downstream the effective gas heating. More generally, the model shows that power-efficient plasma-induced drag reduction requires high plasma heating efficiency.

Nomenclature

C_d	=	net drag coefficient, 1
$\mathcal{D}$	=	drag, N
D	=	front section diameter, m
$D1$	=	main section diameter, m
d	=	spike diameter, m
H	=	power conversion efficiency, 1
h_F	=	fuel mass enthalpy, $\mathrm{J \cdot kg^{-1}}$
I	=	discharge current, A
L_S	=	spike length, m
M	=	Mach number, 1
$\dot{m}$	=	fuel mass flow rate, $\mathrm{kg \cdot s^{-1}}$
N	=	particle density, $\mathrm{m^{-3}}$
n_e	=	electron density, $\mathrm{m^{-3}}$
P	=	flow thermal power flux, $\mathrm{W \cdot m^{-2}}$
P_{IN}	=	discharge input power flux, $\mathrm{W \cdot m^{-2}}$
p	=	pressure, Pa
S_{ref}	=	reference area, $\mathrm{m^2}$
$\mathcal{T}$	=	thrust, N
T	=	temperature, K
T_e	=	electron temperature, $\mathrm{m^{-3}}$
u	=	flow velocity, $\mathrm{kg \cdot m^{-3}}$
V_p	=	discharge voltage, V
α	=	discharge aspect ratio, 1
γ	=	specific heat ratio, 1
Δ	=	bow shock standoff distance, m
Δz	=	shock thickness, m
ε	=	nondimensionalized input power flux, 1
ζ	=	drag reduction ratio, 1
η	=	drag reduction power efficiency, 1
η_p	=	plasma heating efficiency, 1
η_{pe}	=	propulsive efficiency, 1
λ_D	=	Debye length, m
μ_e	=	electron mobility, $\mathrm{m^2\ s^{-1}\ V^{-1}}$
ρ	=	volumetric mass, $\mathrm{kg \cdot m^{-3}}$

Subscripts

st	=	stagnation conditions
0	=	conditions upstream of the shock front
1	=	conditions downstream of the shock front
2	=	conditions downstream of the conical shock

I. Introduction

THE effect of nonequilibrium gas discharges on supersonic airflows has been thoroughly investigated since the early 1990s [1,2]. In particular, the interaction of plasmas with shock waves has been studied using shock tubes [3,4]. In these experiments, shock waves are propagated through ionized gas. Earlier results indicated a strong effect of the discharge on the shock front. In some cases, anomalous shock propagation and shock splitting were observed [5,6]. Macheret et al. [4] observed these effects in Ar-N_2 mixtures at 50 torr and proved that inhomogeneous gas heating of the gas by the plasma can explain these effects. Adamovich et al. [7] studied the propagation of shock wave in ionized gases and demonstrated that double layer formation on the shock front is theoretically possible. Bletzinger and Ganguly [3,8] experimentally demonstrated that a strong electrical double layer is formed by a shock front propagating in a nonequilibrium N_2 discharge. This effect was seen with direct current (dc) discharges or dielectric barrier discharges (DBD). Because unconstrained dc discharges require lower pressure, the use

Received 24 October 2006; revision received 22 March 2007; accepted for publication 27 March 2007.

*Ph.D. Student, Département d'Aérodynamique Fondamentale et Expérimentale (DAFE); pelias@onera.fr. Student Member AIAA.
†DAFE Deputy Director, Département d'Aérodynamique Fondamentale et Expérimentale.
‡Senior Scientist, Département Mesures PHysiques (DMPH).
§Research Scientist, Département Mesures PHysiques (DMPH).

of a DBD allowed the authors to observe this phenomenon at pressures up to 50 torr. The authors underline that strong double layers lead to enhanced electron excitation localized on the shock front and possibly to strong neutral heating.

These results suggest that plasma heating effects might have a significant impact on shock waves. In particular, Bletzinger and Ganguly suggest that double layers could produce very localized energy depositions. They also speculate that this mechanism could significantly alter the shock front.

Thus, to study this phenomenon and evaluate the heating hypothesis, it is necessary to generate a shock-induced plasma double layer in conditions suitable for a careful investigation. Blowdown wind tunnels are able to generate steady bow shock in front of test models. Consequently, one should look forward to obtaining similar double layers on steady shock front generated in a wind tunnel. Indeed, many studies have been devoted to the generation of plasma in supersonic airflow, using different model geometries [1,9–16]. In particular, the nonequilibrium plasma supersonic wind tunnel at the Ohio State University [10,11] allows one to generate dc or RF plasmas upstream of a sharp model. In these studies, strong light emission at the shock front generated by a $M = 3$ supersonic flowing afterglow have been detected, suggesting that a double layer could form at the shock front. These results suggest that supersonic wind-tunnel experiments are appropriate to study the interaction between a plasma and a shock front. However, in this experiment, the discharge is generated upstream of the model. This requires an insulated experimental setup. Besides, the setup is not representative of in-flight conditions because the electrodes must be located upstream of the model. Consequently, the goal of this study is to further investigate the interaction between onboard generated gas discharges and a shock front in a Mach 3 airflow. Thus, experiments are run in a Mach 3 blowdown wind tunnel with a model whose design has been tested by Kuo and Bivolaru [15]. It consists of a blunted geometry designed to generate onboard discharges. The results suggest that the formation of a steady double layer on the bow shock is plausible, and that the discharge input power can be significant. Nevertheless, no effects on the drag are measured. Consequently, to investigate theoretically the effect of a localized heat deposition and to understand why no effect is measured in the experiment, a heat deposition model is proposed.

In the next section, experiment details are given. Sections III and IV present the experimental investigation results and a discussion of these results, respectively. Section V presents the theoretical investigation.

II. Experimental Setup

Experiments are run in the ONERA R1Ch blowdown wind tunnel. The facility delivers a $M = 3$ airflow for 10–30 s, with stagnation pressures ranging from $p_{st} = 0.8 \times 10^5$ Pa to $p_{st} = 3 \times 10^5$ Pa. The stagnation temperature is about $T_{st} = 340$ K. Stagnation conditions are probed with a pressure sensor and a thermocouple. The steady shock front is generated using a test model, as sketched in Fig. 1. It consists of a 30 deg truncated cone with a spike mounted on the front section of diameter $D = 35$ mm and main section of diameter $D1 = 70$ mm. The spike has a 30 deg conical tip. Its length is noted as $L_S = 14$ mm, and its diameter as $d = 5$ mm. To investigate plasma effects on the whole shock system, the model is mounted on a six-component balance, giving, in particular, the drag force with a 1% relative accuracy. The base pressure is considered to be constant on the base surface. It is measured with two pressure probes located near the base. Knowing the base area, the base drag coefficient is computed and subtracted to the measured drag coefficient, yielding the net drag coefficient. The shock features are observed using a schlieren imaging system, sensitive to vertical density gradients. The central spike and the outer shell also play the role of electrodes, with the outer shell being grounded. The central spike is biased to a negative voltage, using a self-regulated dc power supply built by TECHNIX S.A. On the high voltage (HV) line a $R = 10$ kΩ serial resistor is set to avoid current surges. In either case the output current or voltage can be set using 0–10 V command signals. DC current and

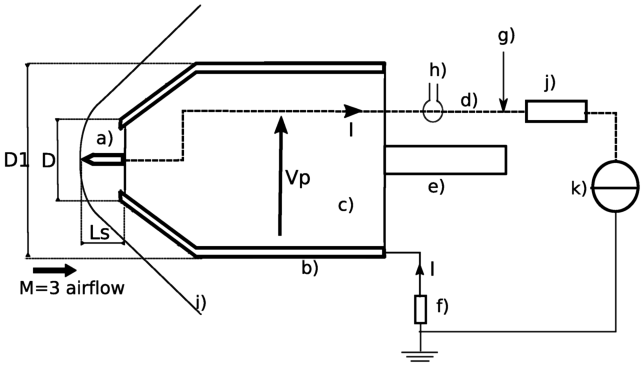

a) Central spike/ Electrode
b) Outer shell / Grounded electrode
c) Ceramic insulation
d) High voltage line
e) Six-component balance
f) 50 Ohms resistor
g) High voltage probe
h) Pearson coil
i) Bow shock
j) Serial resistor
k) dc power supply

Fig. 1 Test model.

voltage probes are built in the power supply. Their sensitivity is quite low; thus the confidence intervals for current and voltage are 5 mA and 100 V around the measured value, respectively. In some cases, fast voltage and current measurements are performed. The discharge voltage is measured with a Northstar PVM-12 high voltage probe. Its bandwidth is between 0 and 80 MHz. The current is measured with a 50 Ω resistor on the grounded side (see Fig. 5) and also with a Pearson Electronics coil on the high voltage line, whose bandwidth is between 200 Hz and 35 MHz. Its rise time is around 10 ns. Because of electric noise, the 95% confidence intervals are 90 V for the HV probe and 0.6 mA for the 50 Ω resistor. The probe signals are recorded on a LeCroy digital oscilloscope, with a 200 MHz sampling rate. Fast measurements have been performed with a $R = 100$ kΩ serial resistor.

For each run, the airflow properties are set by choosing the stagnation pressures p_{st}. The freestream volumetric mass ρ_0, temperature T_0, and particles density N_0 are computed from the stagnation conditions using the standard isentropic relations for $M = 3$ [17]. Without the discharge, and with no central spike, the model generates a detached bow shock. In the vicinity of the model's axis, the shock can be approximated as a plane. In this case, the density ratio before and after the shock is $\rho_1/\rho_0 = 3.85$. The shock standoff distance Δ is measured on the schlieren pictures, giving $\Delta/D = 0.4$. For all the runs reported here, the spike length L_S is equal to Δ. Thus, it does not disturb the steady shock front, but brings near the shock front region the high-intensity electric field generated at its tip. Behind the bow shock, the airflow is more dense. Thus, the reduced electric field E/n is appreciably decreased here.

During a given run, the power supply is turned on when the flow has reached its steady-state conditions. The power supply output current increases linearly, from 0 to I_{max}, in 5 s. The stagnation pressure and stagnation temperature during this period are constant within 5%. A 25-fps digital video camera and a digital camera record the discharge evolution. When discharges images and schlieren images are recorded in the same run, the schlieren lighting system does not allow one to have the same line of sight. In this case, the line of sight of the cameras for visible imaging is not perpendicular to the model axis.

III. Results

A typical current-voltage characteristic recorded during a run is presented in Fig. 2. Stagnation conditions are $p_{st} = 1.1 \times 10^5$ Pa, $T_{st} = 337$ K, giving $p_0 = 3 \times 10^3$ Pa and $T_0 = 120$ K. Three different regimes can be seen, and the pictures of the discharge corresponding to these regimes are given in Fig. 3 with the corresponding schlieren images. Note that visible and schlieren imaging are not synchronized. The trigger signal of the digital camera used in the schlieren system allows one to determine the

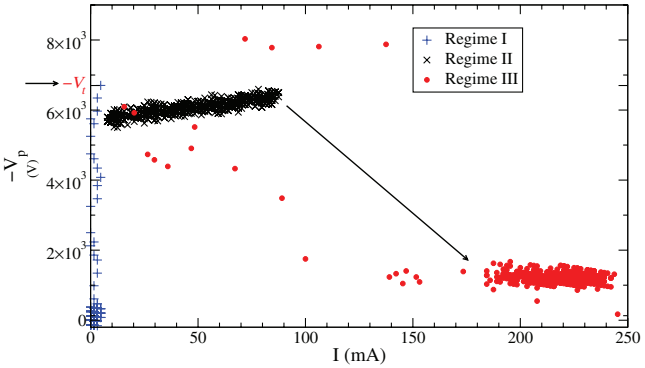

Fig. 2 Discharge current-voltage characteristic, $N_0/N_l = 0.067$, negative spike.

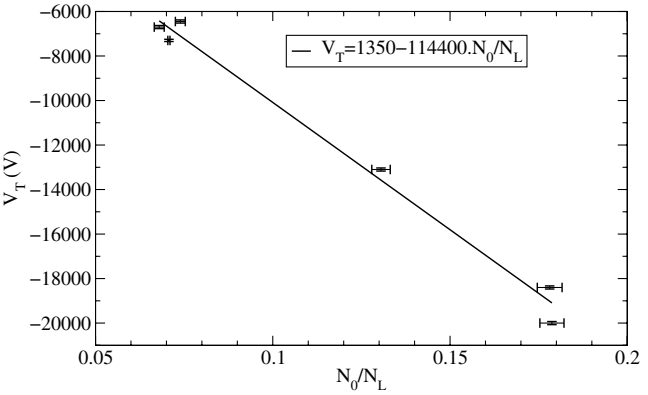

Fig. 4 Transition voltage for negative spike discharge.

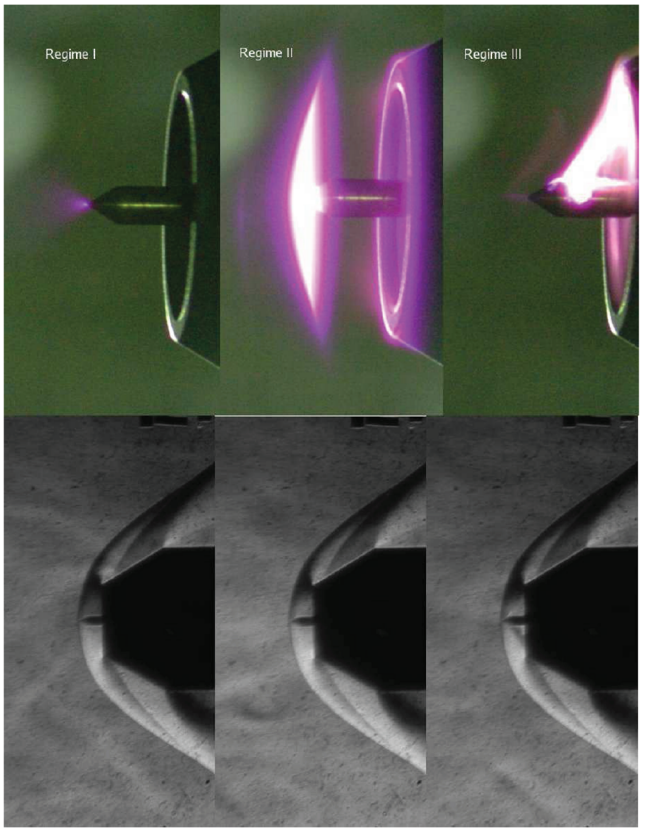

Fig. 3 Discharge pictures (exposure 12, 5 ms) and schlieren (exposure 0, 25 ms) for the different regimes given in Fig. 2.

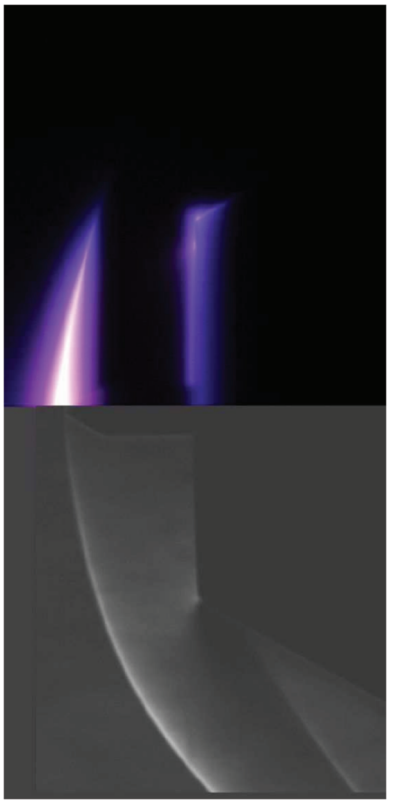

Fig. 5 Superimposition of a discharge view (top, exposure time 25 ms) and a schlieren (bottom, exposure time 10 μs), $N_0/N_L = 0, 106$, $T_0 = 116$ K.

regime during which the images are taken. In the low current region (<5 mA, regime I), a steep slope of the current voltage curve is noticed, corresponding to a high impedance discharge. In this case, we observed a diffuse discharge upstream of the spike tip. The built-in current probe is not sensitive enough to provide an accurate measurement. Measurements using fast response time current probes indicate that the current is formed by repetitive pulses, as shown in Fig. 6b. When the current is increased, at $I = 5$ mA and for a transition voltage $V_p = V_t = -6.7$ kV, the discharge switches to a low impedance regime. Then the voltage magnitude slowly increases with the current. In this case, the peak input power at $I = 80$ mA is $P_{\text{IN}} = 580$ W. Here the discharge is brighter and circular, with a diameter roughly equal to D. The schlieren images in these two cases are identical to the case with no discharge. If the discharge current is increased, the current-voltage characteristic becomes oscillatory, then reaches a very low impedance regime, where the voltage magnitude decreases with the current. Visually, it corresponds to a bright filament between the spike and the grounded shell. It is also possible to set the commanding current constant. In this case one obtains a steady discharge during the whole run.

The transition voltage V_t can be measured for different stagnation conditions. It corresponds to the point where the high impedance corona discharge switches to a low impedance regime (arrow in Fig. 2). Figure 4 gives the measured transition voltage versus freestream particle density N_0, given in fraction of the Loschmidt number ($N_l = 2.687 \times 10^{25}$ m^{-3}). For $N_0/N_l = 0.17$, we measure $V_t = -18$ kV. In this case, the equivalent pressure at $T_0 = 293$ K is 137 torr. With increasing density, the absolute value of the transition voltage V_t increases linearly with the freestream density N_0.

In Fig. 5, a view of the discharge in regime II is superimposed on a schlieren picture of the bow shock generated by the model. To have the same line of sight in both cases, the pictures were taken during two separate runs, with the same flow conditions. Thus proportions are respected. The bow shock is outlined by the lighter region. The discharge is axisymmetric. It is located near the spike tip, slightly in front of the shock wave where the electric field is more intense. It also

seems to follow the curved shock front, because light is emitted along the shock front. When the current is increased, the light emission is increased and covers the entire bow shock. A weaker emission is noticed, near the grounded electrode. Between this electrode and the bright bow shock region, there is a dark region.

In all runs performed, with the negatively biased spike, no appreciable change in the schlieren or drag recording is noted. For this model, the net drag coefficient is

$$C_d = \frac{D}{(1/2)\rho_0 u_0^2 \cdot S_{\text{ref}}} = 0.868 \pm 0.007 \qquad (1)$$

IV. Discussion

A. Influence of Supersonic Flow Conditions

The experimental results show that steady axially symmetric discharges have been generated, in front of a test model in a $M = 3$ airflow. Tests have also been performed in still air, with a density equal to the freestream density computed from experimental data. In this case, the discharge observed is not symmetric, but follows the high electric field region between the spike and the outer shell, along the truncated front section (Fig. 1). Thus, the discharge features is linked to the density field topology. This is not surprising because breakdown occurs in a region of higher reduced electric field E/N. Because of the shock system, a strong compression increases the density around the spike, favoring breakdown in front of the tip, where the electric field is strong and the density low (Fig. 5).

B. Analysis of the Discharge Regime

Electrical measurements give indications on the discharges. First, in Fig. 2, the transition on the I-V curve from a high impedance regime—regime I—to a lower one—regime II—is characteristic of corona to glow discharge transition. In some cases, fast measurements of the discharge voltage and current have been recorded during this transition, as shown in Fig. 6. The power supply voltage magnitude is increased from −5 up to −9 kV. The discharge voltage follows this increase until it reaches the transition voltage V_t.

In the high impedance regime (regime I), repetitive current pulses are recorded, as shown in Fig. 6. These current pulses are periodic, and their amplitude is roughly constant, around 6–10 mA. These pulses are Trichel pulses [18,19]. They exhibit the classical behavior of "Trichel pulses" [18,19], with a nearly constant amplitude and a voltage-increasing repetition rate, as shown in Fig. 6b. Let us stress that the observation of a classical Trichel corona is not obvious in a $M = 3$ flow. In fact, the flow velocity is of the same order of magnitude as the negative ion velocity. In Trichel pulses, negative ions, being less mobile than the electrons, control the space-charge distribution [19]. Their removal allows the onset of another pulse [20]. Here, the electric field tends to repel the ions upstream of the spike, whereas the flow blows them downstream.

For $V_p = -5$ kV, the average current is small, below the uncertainty of the current measurements. The pulse interval is 23 μs. It decreases when the voltage magnitude increases and reaches 10 μs at $V_p = -6.4$ kV and 7 μs at $V_p = -6.9$ kV. Above this voltage, the pulse frequency becomes irregular, then at $V_p = V_t = -7.3$ kV, the current pulses stop and the average current rises up to 5 mA. This produces a 500 V voltage drop. The mean current keeps increasing up to 20 mA, and a small current pulse can be observed again. Note that the signal of the Pearson coil drops, because its low frequency cutoff is around 200 Hz. So the low frequency component of the discharge current is dampened.

Second, we can see that when the current is increased above 80 mA, the I-V curve drop to a very low impedance regime (Fig. 2, regime III). In this case, the voltage magnitude decreases with the current, which is typical of an arc discharge. Arc discharges strongly heat the gas downstream of the bow shock. The heated region corresponds to the bright filament as shown in Fig. 3. In steady state, the density in the core of the filament drops to equalize the pressure, resulting in a strong density gradient. Thus, in Fig. 3 the filament region can be observed on the schlieren pictures corresponding to

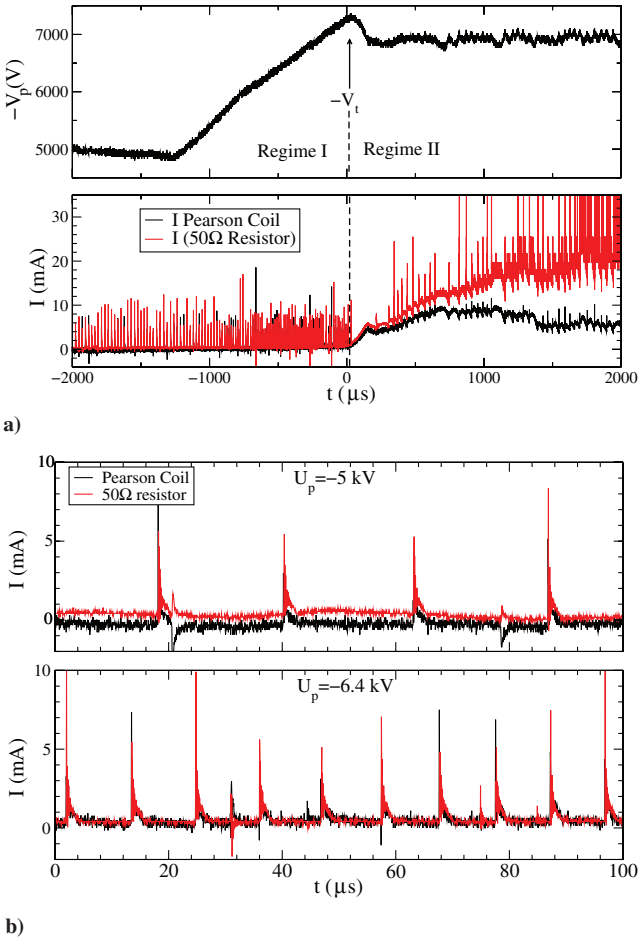

Fig. 6 Discharge voltage and current, measured during the transition from a negative corona regime to a glow regime, for $N_0/N_L = 0.071$. a) Current and voltage during the transition; b) detailed view of the current for two different voltages.

regime III. With enough power, this heating mechanism can be used to create a "fluid body" that can significantly decrease the drag of a body, as shown by Bivolaru in an experimental study [21]. The fact that the low impedance discharge of the regime II can evolve to an arc discharge also supports the fact that regime II corresponds to a glow regime.

Third, the current-voltage characteristic in regime II is slightly increasing. Two hypotheses can be done to explain this increase. On one hand, due to the relatively high pressure downstream of the shock front, the discharge positive column resistivity could be high enough to account for the voltage increase observed in the glow mode. On the other hand, this increase could also suggest that the discharge is an abnormal glow discharge. More precisely, because the electric field is concentrated at the spike tip, it decays rapidly along the spike surface. This decay prevents the discharge from allowing more current to flow by simply extending its cathode region area on the spike. Thus an increase of the cathode current density is also required, and discharges usually do this by enhancing the electric field. Estimates of the cathode current density can be computed by hypothesizing that the cathode region area is conical, and that the base of the cone is the bright step visible in the glow discharges view, as shown in Fig. 3. This area increases with the current and can be computed considering the cone area formula. The current corresponding to these pictures is estimated a posteriori and the current density is given by $j = I/A$. Figure 7 presents the results of this estimation for the conditions given in Fig. 2. The current density tends to increase with the discharge current, which is consistent with an abnormal glow regime. Nevertheless, one cannot decide between these two hypotheses and it is possible that the two phenomena coexist.

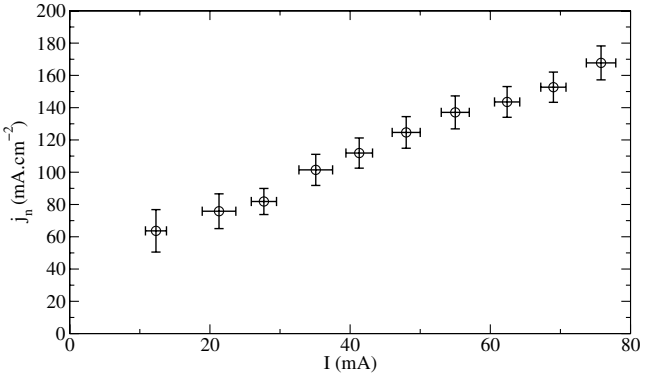

Fig. 7 Current density computed from discharge pictures for the same case as Fig. 2.

These three points suggest that the discharge in regime II is a glow discharge. In addition, two remarks can be made from these data. First, the fast measurement data shown in Fig. 6 provide key elements to explain the transition from the negative corona to the stationary glow discharge. In fact, as pointed out by Akishev et al. [22], the transition occurs when there are enough negative charges in the interelectrode region to build a space-charge electric field high enough to sustain an ionization process. These negative charges are produced by electron attachment on O_2 near the cathode and drift in the electric field toward the anode. Generally, this ionization process starts near the anode. Here, we cannot tell where this charge buildup leading to the transition takes place. In static air, this transition is usually unstable and leads to an arc because ionization instability occurs. However, in our case, the flow velocity is of the same order of magnitude as the drift velocity, delaying the hydrodynamic/ionization instability that yields hot filament arcs.

Second, during the glow regime, the discharge emission patterns are located in the vicinity of the shock and near the anode. There is a substantial dark space behind the shock front. This indicates a low electric field region, where most of the electrons are attached on O_2 molecules. Thus, the neutral excitation by the electrons is weak, resulting in a weak light emission. This also indicates that ionic current could play a significant role in this region to sustain the discharge. The faint visible emission near the anode is the sign of a higher reduced electric field near the anode, possibly because of an anode fall of potential due to a negative charge buildup in this region.

C. Existence of a Double Layer

In this experiment, there is no direct evidence that double layers form at the shock front. However, a few elements suggest that it is effectively the case. First, a strong light emission pattern in the vicinity of the bow shock is observed (see Fig. 5). Though it is not possible to determine whether emission occurs slightly in front of or behind the bow shock, it indicates a strong electron excitation in the region along the shock. In their experiments in shock tubes, Bletzinger et al. also noted a strong light emission in the shock-induced double layers region [3,8]. Siefert [23] also measured an increased light emission and electron density at the shock front propagated in an argon plasma. Secondly, as suggested by Bletzinger et al. [2], a double layer could form across the shock, because its thickness has the same order of magnitude as the Debye length λ_D for electron density $n_e \sim 10^{11}$–10^{12} cm^{-3}. This is because the sharp neutral density gradient across the shock front leads to sharp charged particles density gradient. In this case, diffusive current transport is expected to be dominant across the shock front. According to Raizer ([24], Sec. 2.7.4), charge neutrality is violated if the characteristic length of strong variation of the charge density is of the same order as the Debye length λ_D. Here, the length of variation of this charge density gradient is the shock thickness Δz. If this length Δz is close to the Debye length, this steep gradient cannot be maintained and electrons diffuse upstream of the shock, because electron density is smaller there. Then a volumetric space charge can appear, leading to the formation of a double layer.

The Mott-Smith model [25] gives a shock front thickness $\Delta z = 5.6 \times 10^{-6}$ m for $M = 3$. For an electronic temperature around 2 eV,

$$(\Delta z/\lambda_D)^2 \simeq 3 \times 10^{-13} n_e \tag{2}$$

Thus, if $n_e \leq 10^{13}$ cm^{-3}, then $\Delta z/\lambda_D \leq 1$. In this case, the formation of a double layer across the shock front is plausible. Note that setting $T_e \simeq 2$ eV simply models the fact that few electrons have kinetic energy in the [2; 5 eV] range because of the large N_2 vibrational cross section, and that hotter electrons with a kinetic energy above 5 eV do not contribute to the Debye screening.

V. Heat Deposition Model

The goal of this section is to investigate the effect of a localized heating of the gas in the shock front. As mentioned earlier, despite a relatively high input power in the discharge and a strong light emission near the shock front, indicating that a double layer formation is plausible, no appreciable change of the drag is recorded. So the point is to know whether a noticeable thermal effect of the plasma on the shock front and on the drag can reasonably be expected. For this purpose, modified Rankine–Hugoniot (MRH) jump relations are derived, taking into account a thermal energy release in or around the shock front, in a perfect gas. MRH jump relations give the evolution of the temperature, density, and Mach number across a planar shock in a given Galilean referential. They can model either a shock propagating at uniform velocity in a still medium or a standing shock in front of a blunted body. Adamovich et al. [7] previously proposed a similar derivation to study propagating adiabatic double wave shock systems. Here we focus on the case of a single standing shock in front of a blunt body. The computations give explicit expressions for the downstream Mach number M_1, the density, pressure, and temperature ratios, as a function of the upstream Mach number M_0 and the relative input power flux $\varepsilon = P_{\text{IN}}/P_0$, where P_{IN} is the power flux due to the source term and $P_0 = \rho_0 u_0 c_P T_0$ is the upstream thermal power flux. The details of this derivation are given in Appendix A:

$$M_1 = M_1(M_0, \varepsilon) \qquad \frac{T_1}{T_0} = \frac{1 + \varepsilon + \frac{\gamma-1}{2} M_0^2}{1 + \frac{\gamma-1}{2} M_1^2} \qquad \frac{p_1}{p_0} = \frac{1 + \gamma M_0^2}{1 + \gamma M_1^2} \tag{3}$$

In the present model, no information on the energy source term location is needed. Formally, there is no difference in the jump relation results if the energy is deposited slightly upstream, inside or slightly downstream of the shock. The key parameter is the volumetric source term integrated across the shock, that is, the input power flux. The problem has a physical solution as long as ε is lesser than a critical value $<\varepsilon^*(M_0, \gamma)$, whose expression is given by

$$\varepsilon^* = \frac{1}{2(\gamma + 1)} (M_0 - 1/M_0)^2 \tag{4}$$

For $\varepsilon = \varepsilon^*$ the flow downstream of the shock is sonic. It corresponds to the Chapman–Jouguet point in the detonation theory [26]. Thus, there is a critical power flux, above which this model is inapplicable. If $\varepsilon > \varepsilon^*(M_0)$, the steady-state hypothesis is no longer valid. The shock front velocity will increase until the upstream Mach number reaches a value high enough so that $\varepsilon = \varepsilon^*(M_0')$.

Figure 8 gives the behavior of the downstream Mach number M_1, and the pressure and temperature ratios versus ε. As shown in Fig. 8, the effect of the energy deposition is to decrease p_1 while increasing T_0. As long as $\varepsilon < \varepsilon^*(M_0)$, the solution is completely steady, and the shock front velocity (or equivalently the upstream Mach number) is unchanged.

A crude estimate of the drag of a blunt model of section S_{ref} can also be computed. The bow shock generated by the blunt body is modeled by a planar shock having the same section as the truncated face and a conical shock whose angle is given by the conical shock theory. The pressures behind the planar shock and behind the conical shock are p_1 and p_2, respectively. If D is the truncated section diameter and $D1$ the main section diameter (see Fig. 1), the expression for drag $\mathcal{D}$ is given by

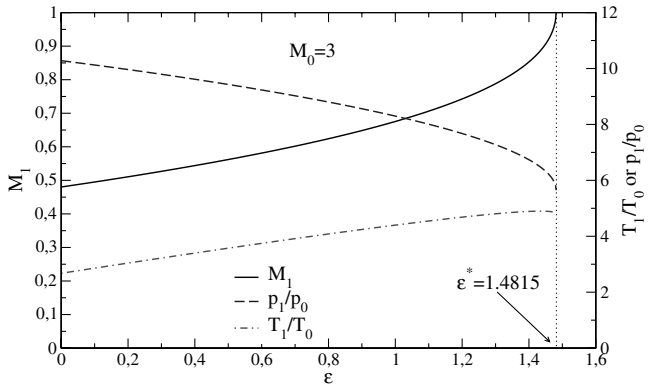

Fig. 8 Downstream Mach number, pressure, and temperature ratios evolution versus the reduced input power flux ε.

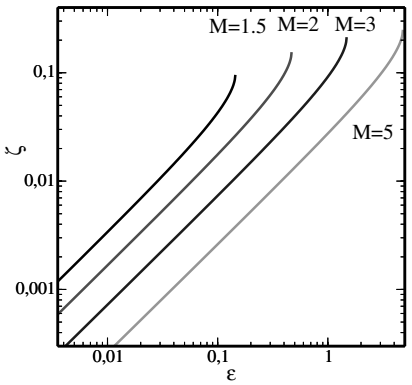

Fig. 9 Drag reduction ratio, for different Mach number, with $\alpha = 0.5$.

$$\mathcal{D} = p_1 \pi \frac{D^2}{4} + p_2 \pi \left(\frac{D1^2 - D^2}{4} \right) \tag{5}$$

The drag coefficient is given by

$$C_d = \mathcal{D} \Big/ \left(\frac{\gamma}{2} p_0 M_0^2 \pi \frac{D1^2}{4} \right)$$

Thus,

$$C_d = \frac{p_1 \pi D^2}{\frac{\gamma}{2} p_0 M_0^2 \pi D1^2} + \frac{p_2 \pi (D1^2 - D^2)}{\frac{\gamma}{2} p_0 M_0^2 \pi D1^2} \tag{6}$$

The conical shock theory gives a shock angle of 42 deg at $M = 3$ for a 30 deg deflection angle, yielding $p_2/p_0 = 3.552$. To compute the drag coefficient in Eq. (6) on a larger Mach number range, it is necessary to use a value for $p_2(M_0)$ taking into account the conical shock angle variation with the Mach number. This is obtained through a simple interpolation of the value given by the conical shock theory. The interpolation p_2/p_0 is given in Appendix B.

With no energy deposition, $p_1/p_0(\varepsilon = 0) = 10.33$, and $C_d = 0.901$. This estimate of the drag is fairly good. This is not surprising because in this setup the pressure levels are mostly dictated by the shock intensity and the friction force is nearly negligible. We define the aspect ratio as $\alpha = D/D1$. If the heating source is located on the standing shock section only, the drag variation $\Delta\mathcal{D}$ due to the heat deposition in the shock on the section S can be estimated by computing

$$\zeta = \frac{\Delta\mathcal{D}}{\mathcal{D}} = \frac{p_1(M_0, \varepsilon) - p_1(M_0, 0)}{p_1(M_0) + p_2(M_0)(1/\alpha^2 - 1)} \tag{7}$$

In Fig. 9, the drag reduction ratio ζ is plotted versus the relative power flux, for different Mach numbers. Thus we are able to compute an estimate of the expected drag reduction due to the heating of the gas in the vicinity of the shock front. In our experiments, the discharge power is around 1 kW. A limiting case is to consider that all this input power goes to the heating of the flow. We consider that the discharge heats the gas on a surface given by the bright region in Fig. 5. Thus, the input power flux reads $\varepsilon = 1.5 \times 10^{-1}$, for $\rho_0 = 8.7 \times 10^{-2}$ kg · m^{-3}, $u_0 = 660$ m · s^{-1}, $T_0 = 120$ K, and $c_p = 10^3$ J · K^{-1} · kg^{-1}. The heated surface corresponds to the truncated section of the model whose contribution for the overall drag is predominant. An estimated drag reduction of $\zeta = 1.1\%$ is obtained. However, in the experiment, no drag reduction has been noticed, although the measurement uncertainty is less than 1%. Nishihara et al. [27], using pressure measurements and visible spectroscopy, showed that only 10% of the input power of a dc discharge in a $M = 3$ flow directly heats the gas. In dc discharge, most of the energy delivered to the electrons by the electric field is channeled in the vibrational energy modes. Compared to the flow transit time, this vibrational energy is frozen, because the vibrational translational relaxation time is a few milliseconds for air below 300 K ([28], Chap. 7), whereas the transit time in the vicinity of the shock is lower than a microsecond. Thus, a direct heating power around 10% of the overall input power gives $\zeta = 0.1\%$, below the measurement uncertainty. Thus, we cannot expect to measure a significant drag reduction.

The energetic efficiency of this process can be assessed by considering the power balance of the model with an engine delivering the thrust $\mathcal{T} = -\mathcal{D}$. We introduce the propulsive efficiency of this engine, given by the thrust power over the fuel power:

$$\eta_{\text{pe}} = \frac{|\mathcal{T}| u_0}{\dot{m} h_F} = \frac{|\mathcal{D}| u_0}{\dot{m} h_F} \tag{8}$$

Here $\dot{m}$ is the fuel flow rate and h_F is the fuel heating value, in J · kg^{-1}. This equation shows that for a constant upstream velocity u_0, the drag reduction ratio ζ is also the fuel mass flow rate reduction ratio.

$$\zeta = \frac{\Delta\dot{m}}{\dot{m}} \tag{9}$$

The plasma heating efficiency η_p is also required. If we call $\dot{m}'$ the fuel mass flow rate necessary to power the plasma power supply, we have

$$\eta_p = \frac{P_{\text{IN}}}{\dot{m}' h_F} \tag{10}$$

Thus, the overall power is

$$P = (\dot{m} - \Delta\dot{m} + \dot{m}') h_F$$

This is to be compared to the baseline power $P_b = \dot{m} h_F$. The energetic efficiency of the shock heating is given by

$$\eta = \frac{P}{P_b} = 1 - \zeta(\varepsilon) + \frac{\dot{m}'}{\dot{m}} \tag{11}$$

From Eqs. (6), (8), and (10) and by using $u_0^2 = M_0^2 \gamma r T_0$, Eq. (11) is recast as

$$\eta = \frac{P}{P_b} = 1 - \zeta(\varepsilon) + \varepsilon \frac{\eta_{\text{pe}}}{\eta_p} \frac{\alpha^2}{C_d M_0^2 (\gamma - 1)} \tag{12}$$

The energetic efficiency of the plasma-induced drag reduction is linked to the power conversion efficiency, given by the ratio $H = \eta_{\text{pe}}/\eta_p$. In Fig. 10, η is plotted versus the relative power flux ε for different H. The drag reduction is power efficient if $\eta \leq 1$. The lower η is, the more efficient the process is. Figure 10 shows that η is below unity for a lower value of H. Moreover, the most efficient case corresponds to the critical relative power flux ε^*. From now on, we will set $\varepsilon = \varepsilon^*$ to assess the maximum effect of plasma-induced shock heating.

This model is useful to investigate the efficiency of the plasma-induced drag reduction. For practical purposes, it is interesting to know the highest power conversion efficiency $H_{\max}$ insuring an

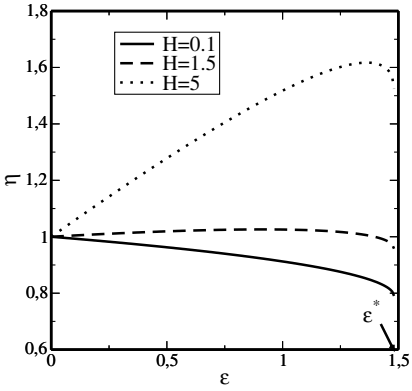

Fig. 10 Energetic efficiency of the drag reduction, for $M = 3$, $\alpha = 0.5$.

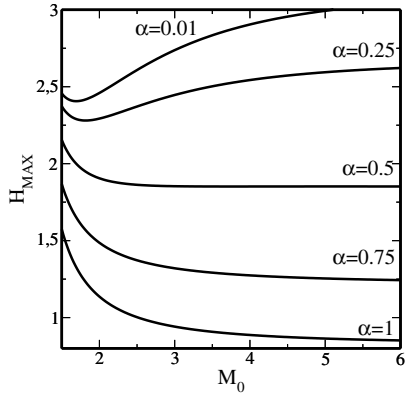

Fig. 11 Maximum power conversion efficiency admissible to achieve efficient plasma-induced drag reduction.

energetic efficiency $\eta \leq 1$. In fact, the higher $H_{\max}$ is, the lower the required plasma heating efficiency η_p can be. Figure 11 gives the value $H_{\max}$ for different aspect ratio α. The value of $H_{\max}$ increases when decreasing the aspect ratio α. Note that in this model, the plasma spatial extension is limited to the truncated section of diameter D. This is justified by the experimental observations, as shown in Fig. 3. Here, the discharge section closely matches the truncated section because of the coaxial arrangement of the electrodes. However, the case $\alpha \to 0$ is not physical because the discharge spatial extension is not equal to zero. Besides, it is possible to imagine a model with a wider, or narrower plasma section, by properly designing a different electrode geometry.

If we set $H = 1$, the plasma-induced drag reduction efficiency can be plotted versus the upstream Mach number, as shown in Fig. 12. When the aspect ratio α vanishes, no power savings are to be expected, because the input power is small. For a given Mach number

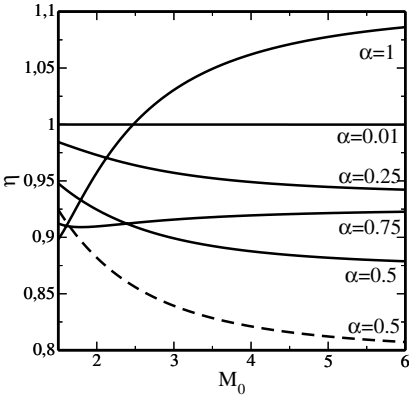

Fig. 12 Plasma-induced drag reduction efficiency, for $H = 1$ (solid line), and $H = 0.5$ (dashed line).

M_0, there is an optimum aspect ratio yielding the maximum drag reduction efficiency. For Mach numbers $M_0 > 2.5$, with $\alpha = 0.5$, power savings up to 10% of the baseline fuel power can be reached. The magnitude of this saving increases when H increases. For instance, for $H = 0.5$, power savings up to 20% can be reached.

These simple computations lead to the following conclusions. First, in our experiment, since around 90% of the input power goes to the vibrational energy modes, the level of drag reduction due to direct heating is beyond the measurement uncertainty of the drag force. Second, a crude estimate of the drag reduction shows that it is possible to efficiently decrease the drag force. For this purpose, the power conversion efficiency $H = \eta_{\text{pe}}/\eta_p$ plays a crucial role. With an optimal aspect ratio α, appreciable power savings are possible if H is low enough.

VI. Conclusions

In this experiment, we have sought to generate steady discharges on a $M = 3$ steady bow shock to assess the possibility of localized gas heating to decrease the drag. The bow shock is generated by a blunted model, with a central spike which is biased to a negative voltage. First, three different discharge regimes have been observed when increasing the discharge current. The first regime corresponds to a high impedance corona regime, the second one to a glow discharge, and the last one to a filamentary arc discharge in the high density volume behind the shock front.

The negative corona regime is formed of Trichel pulses, whose features are classical, despite the high flow velocity. The glow regime is characterized by a low impedance and seems to closely follow the shock front. Behind the shock front, there is a dark space in this regime, possibly indicating an ion rich region. The electrical input power can reach up to $P_{\text{IN}} \simeq 0.5$ kW. We have not observed a noticeable effect of the discharge on the flow and the drag force. We speculate that a double layer could form along the shock front. In fact, the shock front thickness is of the same order of magnitude as the plasma Debye length, for electron density up to 10^{13} cm^{-3}. However, the presence of this double layer in our experiments cannot be clearly proved, so we cannot conclude on the efficiency of double layers to alter the shock front by localized heat deposition.

Finally, to further investigate localized heat deposition effects in the glow mode, modified Rankine–Hugoniot jump conditions have been computed taking into account a heat source. This allows us to compute an estimate of the drag coefficient on the model. If all the electrical input power heated the gas, the drag would be reduced by roughly 1.1%. Because the drag measurements have remained unchanged when turning on the discharges, this points out the fact that only a fraction of the input power heats the gas. Indeed, most of the power goes to the vibrational energy modes. Nevertheless, this simple model shows that drag reduction can actually be achieved when heating the gas. Depending on the power conversion ratio H, plasma-induced drag reduction can lead to appreciable power savings. An efficiency increase requires a lower H. Hence, for a given propulsive efficiency η_{pe}, a high plasma heating efficiency η_p is necessary.

To summarize, the steady glow discharges generated in these experiments follow the bow shock front. They absorb a large amount of power, but do not efficiently heat the gas. Drag measurements are unchanged when turning on the discharge. However, the simple model presented here shows that drag reduction by localized heat deposition is possible. For this purpose, efficient gas heating is required. Recently, Pancheschnyi et al. [29] have shown that repetitive filamentary nanosecond discharges produce rapid air heating if breakdown conditions are met, that is, if the gap conductivity is high enough. The filamentary regime is required to observe this rapid heating of the gas. According to this experiment, the air temperature can increase by a few thousand Kelvins in a few nanoseconds, possibly because of collisional quenching of electronical excited species. Thus, a repetitive nanosecond excitation superimposed to a dc discharge providing the seed electrons could result in rapid heating of the gas. Further experiments will be run to verify this hypothesis.

Appendix A: Derivation of Modified Rankine–Hugoniot Jump Relations

This derivation is similar to the classical RH derivation, except that an energy source term is added on the right-hand side of the energy conservation equation. In this derivation, balance equations for the mass, momentum, and energy fluxes are written over a control volume enclosing the shock front, as shown in Fig. 13 (see [26], Chap. 1).

$$\lfloor \rho u \rfloor_0^1 = 0 \tag{A1}$$

$$\lfloor \rho u^2 + \rho r T \rfloor_0^1 = 0 \tag{A2}$$

$$\left\lfloor \rho u \left(c_p T + \frac{1}{2} u^2 \right) \right\rfloor_0^1 = \int_0^1 S_E \, \mathrm{d}x = P_{\mathrm{IN}} \tag{A3}$$

Here $r = 287\ \mathrm{J\,K^{-1}\,kg^{-1}}$ and S_E is the volumetric heat source, given in $\mathrm{W \cdot m^{-3}}$. Here, P_{IN} is expressed in $\mathrm{W \cdot m^{-2}}$. It corresponds to the power flux due to the energy source term:

$$P_{\mathrm{IN}} = \int_{(0)}^{(1)} (S_E) \, \mathrm{d}x$$

Thus ε is defined as

$$\varepsilon = \frac{P_{\mathrm{IN}}}{P_0}$$

where P_0 is the upstream thermal power flux given by $P_0 = \rho_0 u_0 c_P T_0$. By writing that

$$\frac{p_1}{p_0} = \frac{\rho_1 r T_1}{\rho_0 r T_0}$$

and by using the mass, momentum, and energy balance equations to derive the ratios ρ_1/ρ_0, p_1/p_0, and T_1/T_0, respectively, a fourth order equation in M_1 is obtained. The first one corresponds to a nonshocked system, where $M_1(\varepsilon = 0) = M_0$. The second one corresponds to a shocked solution, given by

$$M_1^2 = \frac{\gamma M_0^4 + 1 - 2\varepsilon\gamma M_0^2 - (1 + \gamma M_0^2)\sqrt{\Delta(M_0, \varepsilon)}}{2\gamma M_0^2(1 + \gamma\varepsilon) - (\gamma - 1)}$$

where

$$\Delta(M_0, \varepsilon) = M_0^4 - 2M_0^2(\varepsilon(\gamma + 1) + 1) + 1$$

To be physically acceptable, we also require that $\Delta(M_0, \varepsilon) \geq 0$. This is true as long as $\varepsilon \leq \varepsilon^*$

$$\varepsilon^* = \frac{1}{2(\gamma + 1)} (M_0 - 1/M_0)^2$$

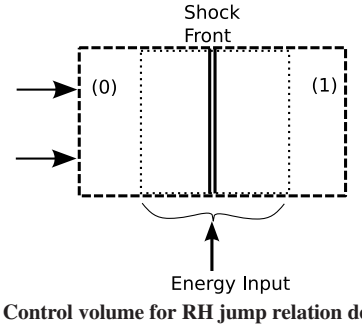

Fig. 13 Control volume for RH jump relation derivation.

When $\varepsilon = \varepsilon^*$, the jump relations are given by

$$M_1(\varepsilon^*) = 1 \qquad \frac{p_1}{p_0}(\varepsilon^*) = \frac{1 + \gamma M_0^2}{\gamma + 1}$$

$$\frac{T_1}{T_0}(\varepsilon^*) = \left(\frac{1 + \gamma M_0^2}{\gamma + 1} \right)^2 \frac{1}{M_0^2}$$

The Hugoniot curve is given by

$$\frac{p_1}{p_0} = \frac{(\gamma + 1) + 2\gamma\varepsilon - \frac{\rho_0}{\rho_1}(\gamma - 1)}{(\gamma - 1) + \frac{\rho_0}{\rho_1}(\gamma + 1)}$$

The solution of the problem is given by the intersection of this curve with the Rayleigh line describing the mass conservation

$$\frac{p_1}{p_0} = 1 - \gamma M_0^2 \left(\frac{\rho_0}{\rho_1} - 1 \right)$$

Hugoniot curves for different values of ε are shown in Fig. 14, as long as the Rayleigh line for $M = 3$. If $\varepsilon = 0$, the problem admits two solutions A_0 and B_0, which corresponds to the classical Rankine–Hugoniot problem. Solution A_0 is the nonshocked solution. When $\varepsilon = 0.5$, the two solutions are A_1 and B_1, the pressure jump across the shock, given by B_1 is decreased. For $\varepsilon = \varepsilon^*$, the Rayleigh line becomes tangent to the Hugoniot curve so that the solutions A_2 and B_2 coincide.

To check whether the solutions given above are physically acceptable, the entropy variation across the control volume has to be positive. The entropy variation across the control volume is given by

$$\Delta s = c_v \, \ell n \left[\frac{p_1}{p_0} \left(\frac{\rho_0}{\rho_1} \right)^{\gamma} \right]$$

By setting $\beta = (p_1/p_0) - 1$, this yields

$$\Delta s = c_v \, \ell n(1 + \beta) + \ell n \left(\frac{1 + \varepsilon + \frac{(\gamma - 1)\beta}{2\gamma}}{1 + \frac{(\gamma + 1)\beta}{2\gamma}} \right)$$

If $\varepsilon = 0$, it is necessary to have $\beta \geq 0$ to have $\Delta s \geq 0$, which means that compression shocks only are physically acceptable. If $\varepsilon > 0$, it is sufficient to have $\beta \geq 0$ to have $\Delta s \geq 0$. However, it is also possible to have $\varepsilon > 0$, $\beta < 0$, and $\Delta s \geq 0$. This is beyond the scope of this paper, because the flow conditions in this study are supersonic. Nevertheless, this means that the flow upstream of the control volume can be subsonic and can be supersonic at the volume outlet.

Appendix B: Conical Shock Pressure Jump Interpolation

The pressure p_2 corresponds to the pressure downstream of the conical shock generated by the conical part of the model. If $\sigma(M_0)$ is the shock angle for a given upstream Mach number M_0, the pressure

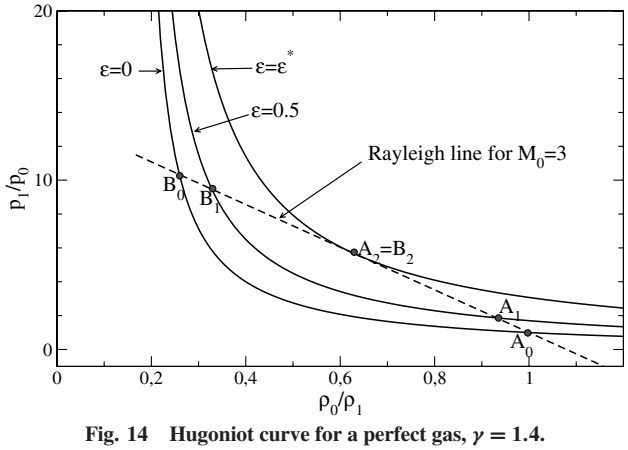

Fig. 14 Hugoniot curve for a perfect gas, $\gamma = 1.4$.

ratio p_2/p_0 is computed with the classical Rankine–Hugoniot jump relations with the normal Mach number $M_{n0} = M_0 \sin(\sigma)$. The angle $\sigma(M_0)$ is given by the conical shock theory. Below $M_0 = 1.5$, no attached shock solution exists. Thus the interpolation is given in the range $1.5 \leq M_0 \leq 6$:

$$\frac{p_2}{p_0} = 0.3109M_0^2 - 0.0808M_0 + 0.9968$$

Acknowledgments

This study is part of the ONERA PUMA ("Plasmas Utiles à la Maîtrise de l'Aérodynamique") research program. The authors would like to thank the wind-tunnel team for its assistance, as well as J. Delery for his insightful comments. Thanks are also extended to C. Laux for his kind assistance.

References

[1] Fomin, V., Tretyakov, P., and Taran, J.-P., "Flow Control Using Various Plasma and Aerodynamic Approaches (Short Review)," *Aerospace Science and Technology*, Vol. 8, No. 5, 2004, pp. 411–421.

[2] Bletzinger, P., Ganguly, B., Van Wie, D., and Garscadden, A., "Plasmas in High Speed Aerodynamics," *Journal of Physics D: Applied Physics*, Vol. 38, No. 4, 2005, pp. R33–R57.

[3] Bletzinger, P., Ganguly, B., and Garscadden, A., "Strong Double-Layer Formation by Shock Waves in Nonequilibrium Plasmas," *Physical Review E*, Vol. 67, No. 4, 2003, pp. 047401–047401-4.

[4] Macheret, S., Ionikh, Y., Chernysheva, N., Yalin, A. P., Martinelli, L., and Miles, R. B., "Shock Wave Propagation and Dispersion in Glow Discharge Plasma," *Physics of Fluids*, Vol. 13, No. 9, 2001, pp. 2693–2705.

[5] Bityurin, V., Klimov, A., Leonov, S., Popov, N., and Van Wie, D., "Shock Wave Structure and Velocity at Propagation Through Non-Homogeneous Plasma," AIAA Paper 2000-2571, June 2000.

[6] Klimov, A., Bityurin, V., and Serov, Y., "Non-Thermal Approach in Plasma Aerodynamics," AIAA Paper 01-16252, Jan. 2001.

[7] Adamovich, I. V., Subramaniam, V. V., Rich, J. W., and Macheret, S. O., "Phenomenological Study of Shock Wave Propagation in Weakly Ionized Plasma," *AIAA Journal*, Vol. 36, No. 5, 1998, pp. 816–822.

[8] Bletzinger, P., Ganguly, B., and Garscadden, A., "Influence of Dielectric Barrier Discharges on Low Mach Number Shock Wave at Low to Medium Pressures," *Journal of Applied Physics*, Vol. 97, No. 11, 2005, pp. 113303–113303-6.

[9] Palm, P., Meyer, R., and Plönjes, E., "Nonequilibrium Radio Frequency Discharge Plasma Effect on Conical Shock Wave: M = 2.5 Flow," *AIAA Journal*, Vol. 41, No. 3, 2003, pp. 465–469.

[10] Merriman, S., Ploenjes, E., Palm, P., and Adamovich, I., "Shock Wave Control by Nonequilibrium Plasmas in Cold Supersonic Gas Flows," *AIAA Journal*, Vol. 39, No. 5, 2001, pp. 1547–1552.

[11] Meyer, R., Palm, P., Ploenjes, E., Rich, J. W., and Adamovich, I., "Nonequilibrium Radio Frequency Discharge Plasma Effect on a Conical Shock Wave: M = 2.5 Flow," *AIAA Journal*, Vol. 41, No. 5, 2003, pp. 465–469.

[12] Shang, J., "Plasma Injection for Hypersonic Blunt-Body Drag Reduction," *AIAA Journal*, Vol. 40, No. 6, June 2002, pp. 1178–1186.

[13] Kolesnichenko, Y., Brovkin, V., Leonov, S., Gorynya, A. A., and Ryvkin, M. I., "Influence of Differently Organized Microwave Discharge on AD-Body Characteristics in Supersonic Flow," AIAA Paper 2001-3060, 2001.

[14] Kuo, S., Kalkhoran, I., Bivolaru, D., and Orlick, L., "Observation of Shock Wave Elimination by a Plasma in a Mach = 2.5 Flow," *Physics of Plasmas*, Vol. 7, No. 5, 2000, pp. 1345–1348.

[15] Kuo, S., and Bivolaru, D., "Plasma Effect on Shock Waves in a Supersonic Flow," *Physics of Plasmas*, Vol. 8, No. 7, 2001, pp. 3258–3263.

[16] Cain, T., and Boyd, D., "Electroaerodynamics and the Effect of an Electrical Discharge on Cone/Cylinder Drag at Mach 5," AIAA Paper 99-0602, Jan. 1999.

[17] Liepmann, H., and Roshko, A., *Elements of Gasdynamics*, 3rd ed., Wiley, New York, 1960.

[18] Cross, J., Morrow, R., and Haddad, G., "Negative Point-Plane Corona in Oxygen," *Journal of Physics D: Applied Physics*, Vol. 19, No. 6, 1986, pp. 1007–1017.

[19] Morrow, R., "Theory of Negative Corona in Oxygen," *Physical Review A*, Vol. 32, No. 3, 1985, pp. 1799–1809.

[20] Reess, T., and Paillol, J., "The Role of the Field-Effect Emission In Trichel Pulse Development in Air at Atmospheric Pressure," *Journal of Physics D: Applied Physics*, Vol. 30, No. 22, 1997, pp. 3115–3122.

[21] Bivolaru, D., and Kuo, S., "Aerodynamic Modification of Supersonic Flow Around Truncated Cone Using Pulsed Electrical Discharges," *AIAA Journal*, Vol. 43, No. 7, July 2005, pp. 1482–1489.

[22] Akishev, Y., Grushin, M., Karal'nik, V., Napartovich, A., and Trushkin, N., "Negative Corona, Glow and Spark Discharges in Ambiant Air and Transitions Between Them," *Plasma Source Science and Technology*, Vol. 14, No. 2, 2005, pp. S18–S25.

[23] Siefert, N. S., "Double Layers and Light Emission at Shock Fronts in Weakly-Ionized Argon," AIAA Paper 2006-3572, June 2006.

[24] Raizer, Y. P., *Gas Discharge Physics*, Springer–Verlag, New York, 1987.

[25] Mott-Smith, H., "Solution of the Boltzmann Equation for a Shock Wave," *Physcial Review*, Vol. 82, No. 6, 1952, pp. 885–892.

[26] Zel'dovich, Y. B., and Raizer, Y., *Physics of Shock Waves and High-Temperature Phenomena*, Academic Press, New York, 1966.

[27] Nishihara, M., Rich, J., Lempert, W. R., Adamovich, I. V., and Gogineni, S., "Low-Temperature M = 3 Flow Deceleration by Lorentz Force," *Physics of Fluids*, Vol. 18, No. 10, 2006, pp. 086101–086101-11.

[28] Capitelli, M., Ferreira, C., Gordiets, B., and Osipov, A., *Plasma Kinetics in Atmospheric Gases*, Springer, Berlin, 2000.

[29] Pancheschnyi, S. V., Lacoste, D., Bourdon, A., and Laux, C. O., "Ignition of Propane-Air Mixtures by a Repetitively Pulsed Nanosecond Discharge," *IEEE Transactions on Plasma Science*, Vol. 34, No. 6, 2006, pp. 2478–2487.

N. Clemens
Associate Editor